Transactions on Energy Systems and Engineering Applications

Article

Performance Enhancement of High Speed Interior Permanent Magnet Synchronous Motors Using Superior Magnetic Material

Tanuj Jhankal[1], and Amit N. Patel[1,*]

[1] Department of Electrical Engineering, Institute of Technology, Nirma University, Ahmedabad, India.
[*] Correspondence: amit.patel@nirmauni.ac.in

Received: 27 March 2023; Accepted: 15 May 2023; Published: 25 May 2023

Abstract: This paper presents the application of higher-grade magnetic material for performance improvement of interior permanent magnet synchronous motors (IPMSM) for high-speed applications. The efficiency and weight of the motor are important performance parameters for high-speed applications. Efficiency improvement with simultaneous weight reduction is the key design issue for many specific applications. The main contribution of this work is to explore the possibility of using high-grade magnetic material for efficiency improvement with a simultaneous weight reduction of IPMSM motors. Three different standard rating motors were designed with the usual M19 material, and their performance was estimated. Finite element modelling and simulation was carried out to validate the initial design. For performance comparison, initial designs were regarded as reference designs. Design improvement was carried out with the application of high-grade magnetic material Hiperco 50A and its influence on the performance of IPMSM motors was analyzed. Three different standard ratings motors were considered in this work to analyze the effect of material in a wide range. Improved design was also validated with finite element modelling and simulation. It was observed that the efficiency is effectively improved with weight reduction using Hiperco 50A material in all three standard-rating IPMSM motors.

© 2023 by the authors. Published by Universidad Tecnológica de Bolívar under the terms of the Creative Commons Attribution 4.0 License. Further distribution of this work must maintain attribution to the author(s) and the published article's title, journal citation, and DOI. https://doi.org/10.32397/tesea.vol4.n1.505

1. Introduction

Permanent magnet synchronous motors (PMSM) are widely used for applications such as electric vehicles, submersible pumps, aerospace, industrial, and domestic applications due to better efficiency, fast dynamic response, wide speed range, and compact size [1]. Fast development in the field of permanent magnet machines is expected to continue due to development in permanent magnet technology, semiconductor devices, and manufacturing techniques. Moreover, compared with other motor structures, PMSM has the advantages of diverse stator and rotor structures and characteristics of good control.

How to cite this article: Jhankal, Tanuj; Patel, Amit N.. Performance Enhancement of High Speed Interior Permanent Magnet Synchronous Motors Using Superior Magnetic Material. *Transactions on Energy Systems and Engineering Applications*, 4(1): 505, 2023. DOI:10.32397/tesea.vol4.n1.505

Therefore, PMSMs are more widely used in high-speed fields [2]. Permanent magnet synchronous motors have very wide application prospects. Optimized efficiency and weight of the motor are the two most desirable performance criteria for machine designers. It is essential to enhance efficiency with weight reduction during motor design. When operating at high speed, the loss density of the permanent magnet motor is much higher than that of low and medium-speed motors. This is primarily due to the generation of stator core loss and large copper loss caused by the high-frequency alternating magnetic field and high-frequency alternating current in the stator, respectively. To overcome this problem, it is necessary to be more careful in the choice of materials compared to conventional motors [3, 4]. The magnetic properties and the weight of any magnetic material significantly influence the power density and efficiency of the machines [5, 6]. High-efficiency motors with superior dynamic performance considerably improve the overall performance and reduce the energy consumption of the entire system [7]. This type of motor is becoming a major point of interest for designers due to the accessibility of high-energy density rare earth permanent magnets and developments in semiconductor devices [8–10].

When designing high-speed permanent magnet motors, selecting stator and rotor structures and materials is of utmost importance. The performance of high-speed PMSM is highly dependent on the magnetic properties of the core material [11]. In this work for initial designs, M19, 29Ga cold-rolled silicon steel laminated sheet stack was used for the magnetic core of the stator as well as the rotor side assembly. Since M19 offers almost the lowest core loss in this class of material and only has a minor cost impact, M19 is probably the most popular grade for motion control products [12]. For cost-effective and average performance M36 or M45 is commonly used with a lamination thickness of 0.5 mm. These laminations are readily available in the market. However, M19 cold-rolled silicon steel material is used as core material in designing different rating motors to achieve a reduced core loss component in the designed motors. With the objective of performance improvement, superior magnetic material Hiperco 50A is used as the core material. The Hiperco 50A material exhibits obvious advantages in several aspects. Hiperco 50A is a typical Co-Fe alloy for electric machines with a specific composition of 49% iron, 49% cobalt, and 2% vanadium (FeCoVa), providing a high magnetic saturation ($2.3 - 2.4$ T) that is greater than that of the M19 material's magnetic saturation point. Hiperco 50A also offers low core losses that can contribute to improving the efficiency of PMSM [13]. To achieve the required mechanical strength of the material while minimizing iron losses and maximizing magnetic permeability, there are a few factors that can be tweaked. One way to do this is by adjusting the ratio between cobalt and iron content in the alloy. Another option is the temperature cycle, during the annealing process, it can be changed to achieve the desired results. And it can also be achieved by adding niobium to the alloy mixture [14]. Several studies have identified alloy of iron-cobalt-vanadium as a potential candidate to increase the specific power of synchronous reluctance machines (SRM) [15] and permanent magnet synchronous machines [16] for high-speed and aircraft applications. In wind power generator application, Ramkumar and Latha [17] have presented that the power density of switched reluctance generator (SRG) increased with an increase in flux density (Bm), using different core materials and concluded that to develop an SRG with higher efficiency, reduced losses, increased power density, and torque material selection is crucial. M. E. Abdollahi et al. presented the design of a high-density SRM for an aerospace application and proposed a multi-objective optimization framework for the design of a high-power density SRM [18]. However, some reports state an increment in specific torque/power by 20% while using FeCoVa alloys for applications like specialized electric and hybrid systems in motorsport applications [19]. $^{R-I}$Sourcing and procuring Hiperco 50A material is not an issue currently for motor designers but Hiperco 50A lamination costs more than M19 due to post-processing needs and cobalt content [20]. Hence, the use of Hiperco 50A is justifiable in the case of high-performance applications demanding very high speed, high efficiency, small size, and less weight.

Design of IPMSM for the high-speed application requires additional factors that must be taken into account compared to conventional low and medium-speed motors. It is important to consider these factors to ensure optimal performance. This paper delves into the comparison between the traditional core material and superior core material, the selection process and proposes the performance improvement of high-speed IPMSM. Efficiency and weight are key performance parameters in high-speed applications. The novelty of this work comprises efficiency improvement and weight reduction simultaneously with the application of superior magnetic material, i.e. Hiperco 50A in place of M19 material. The proposed technique neither change topology nor increases manufacturing complexity; hence it is implementable and viable. Initially, three different standard rating reference motors are designed, and the design information is used for electromagnetic field analysis. The electromagnetic field analysis establishes the correctness of the initial designs. Section II presents the initial design information of three different standard rating IPMSMs, which includes the motor ratings, type of material used, type of motor topology and other design considerations. The design of IPMSM with the use of Hiperco 50A material is presented in section III. Section IV discusses the effect of using Hiperco 50A material on the overall performance of three motors. Comparative performance analysis is carried out between reference motors and improved motors with the application of Hiperco 50A in place of the M19 silicon steel stator magnetic core. While section V concludes the work presented in the paper.

2. Initial Design of IPMSM

The IPMSM design mainly involves four major steps: (i) determination of main dimensions, (ii) stator design, (iii) rotor design and (iv) performance estimation. Various design variables like magnetic loading, slot-loading, space factor, winding factor, aspect ratio, split ratio, conductor current density, magnet fraction and core flux density are selected appropriately considering materials availability and performance requirements [21]. Usually, magnetic loading is assumed between 0.4 T to 0.9 T, and slot-loading is assumed between 100 to 400 A. The range of conductor current density is $4\mathrm{A/mm^2}$ to $8\mathrm{A/mm^2}$, and the magnet fraction is 0.67 to 0.9 [22].

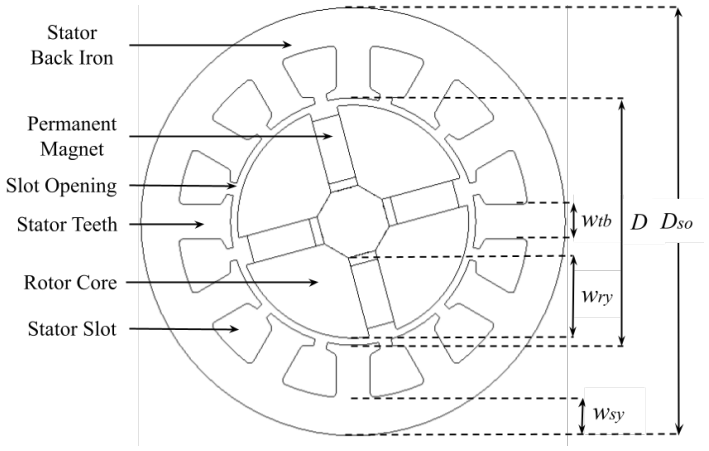

Figure 1. Coss-sectional view of a typical radial-flux inner rotor spoke-type IPMSM.

The cross-sectional view of a typical spoke-type IPMSM is given in Figure 1 for a better understanding of the spoke-type permanent magnet rotor and slotted stator's physical arrangement along with the geometrical design parameters. The main dimensions of IPMSM have been calculated, with the assumption of L/D ratio [23], as follows:

$$D^2L = \frac{P}{11\eta_o cos\phi B_g ack_w n10^{-3}} \quad , \tag{1}$$

where P is the power rated, D the bore diameter, L the axial length of the motor, η_o the assumed efficiency, $cos\phi$ the power factor, B_g the air-gap flux density, ac the electrical loading, and k_w the winding factor. The width of stator yoke (w_{sy}), stator teeth (w_{tb}) and rotor yoke (w_{ry}) can be determined from

$$w_{sy} = \frac{\pi R_{ro} B_g}{N_m k_{st} B_{sy}} \ , \tag{2}$$

$$w_{tb} = \frac{2\pi R_{ro} B_g}{N_{sm} k_{st} B_{st}} \ , \tag{3}$$

and

$$w_{ry} = \frac{\pi R_{ro} B_g}{N_m k_{st} B_{ry}} \ , \tag{4}$$

where R_{ro} is the rotor outer radius, N_m the number of poles, B_{sy} the assumed flux density in stator yoke, N_{sm} the number of slots per pole, B_{st} the assumed flux density in stator teeth, B_{ry} the assumed flux density in rotor yoke, and k_{st} is the stacking factor. Magnetic flux density in the respective section is assumed based on expected performance, and the permanent magnet's thickness is calculated from the following equation:

$$B_g = \frac{F_{lkg} C_\phi B_r}{1 + \left(\mu_{rec} \times C_\phi \times \frac{l_g}{l_m}\right)} \ , \tag{5}$$

where F_{lkg} is the flux leakage factor, B_r the remanence of the permanent magnet, C_ϕ the flux concentration factor, l_g the air-gap length, l_m the thickness of permanent magnet, and μ_{rec} the recoil permeability of permanent magnet. The efficiency of IPMSM can be estimated from various losses like copper loss, iron loss, friction and windage loss, stray loss and permanent magnet loss. Equations for various losses are derived in terms of design variables and motor dimensions. Considering the assumed design variables, design details and motor, efficiency η can be calculated as

$$\eta = \frac{P}{P + P_{loss}} \ , \tag{6}$$

and total loss P_{loss} is given by

$$\begin{aligned} P_{loss} &= P_{cu} + P_i + P_{fw} + P_{stray} + P_{pm} \\ &= \left[N_{ph} I_{ph}^2 R_{ph}\right] + \left[\rho_{bi} V_{st} P_{sp}\right] + \left[P_{fw}\right] + \left[P_{stray}\right] + \left[P_{pm}\right] \\ &= \left[N_{ph} I_{ph}^2 N_{sp} \left\{\left(\frac{\rho n_s^2 L}{k_{cp} A_s}\right) + \left(\frac{\rho \pi \tau_c n_s^2}{2 k_{cp} A_s}\right)\right\}\right] \\ &\quad + \left[\rho_{bi} P_{sp} \left\{\left(\pi \left(R_{so}^2 - R_{si}^2\right) - N_s A_s\right) \times L k_{st}\right\}\right] \\ &\quad + \left[\frac{1}{2} C_f \rho_r \left(\pi n^3\right) \left(D_o^5 - D_i^5\right)\right] + \left[P_{cu} \left(k_d - 1\right)\right] + \left[\frac{V_{pm} w_{pm}^2 B_g^2 \omega^2}{12 \rho_{pm}}\right] \ , \end{aligned} \tag{7}$$

where P_{cu} is the copper loss, P_i the iron loss, P_{fw} the friction and windage loss, P_{stray} the stray loss, P_{pm} the permanent magnet loss, N_{ph} the number of phases, A_s the slot cross-sectional area, I_{ph} the phase current, R_{ph} the phase resistance, ρ_{bi} the mass density (kg/m^3) of back iron, V_{st} the stator volume, P_{sp} the specific iron loss, τ_c the coil-pitch factor, n_s the turns per slot, N_{sp} the slots per pole, $\rho = 1.72 \times 10^{-8} (\Omega - m)$ is the resistivity of copper, k_{cp} is the conductor packing factor, R_{si} the stator inner radius, R_{so} the stator outer radius, N_s the number of slots, C_f the friction coefficient, k_d the ratio of effective AC resistance versus DC resistance, ω the frequency, V_{pm} the volume of permanent magnet, w_{pm} the permanent magnet width, and $\rho_{pm} = 1.5 \times 10^{-6} \ (\Omega - m)$ is the resistivity of a permanent magnet (NdFeB).

The weight of IPMSM includes the weight of the stator core, stator teeth, rotor core, permanent magnet and copper winding. The weight of various motor sections is derived in terms of design variables and motor dimensions. The following equation is derived to estimate the weight (W_{total}) of IPMSM in terms of various design variables, design details and motor dimensions:

$$\begin{aligned} W_{total} &= W_{sc} + W_{st} + W_{rc} + W_{pm} + W_{cu} \\ &= \left[\rho L k_{st} \pi \left\{\left(R_{so}^2 - R_{sb}^2\right)\right\}\right] + \left[\rho_{st} L k_{st} \pi \left\{\left(R_{sb}^2 - R_{si}^2\right) - N_s A_s\right\}\right] \\ &+ \left[\rho_{rc} L \pi \left\{\left(R_{ro} - l_m\right)^2 - R_{ri}^2\right\}\right] \\ &+ \left[\rho_M L \pi \left\{\left(R_{ro}^2 - \left(R_{ro} - l_m\right)^2\right)\right\}\right] + \left[0.5 L_{mt} \rho_{cu} N_s Z_{ss} a_c\right] \quad , \end{aligned} \tag{8}$$

where W_{sc} is the weight of stator core, W_{st} the weight of stator teeth, W_{rc} the weight of rotor core, W_{pm} the weight of permanent magnet, W_{cu} the weight of copper winding, ρ_{sc} the mass density (kg/m^3) of stator core, L_{mt} the length f mean turn, Z_{ss} the conductors per slot, R_{ri} the rotor inner radius, a_c the sectional area of conductor, ρ_{cu} the mass density of copper, and ρ_M is the mass density of permanent magnet.

Figure 2 illustrates the flowchart for the computer-aided design (CAD) of IPMSM. Computer-aided design of IPMSM includes a database of various materials, a selection of design variables, performance estimation and decision-making loops for performance checks. The performance of the motor is estimated according to the calculated dimensions, material properties and assumed design variables [24]. It takes corrective actions if estimated performance deviates from expected performance.

Three standard rating IPMSMs of 2 kW, 200 000 rpm; 5 kW, 24 000 rpm and 120 kW, 10 000 rpm are initially designed using M19 cold-rolled silicon steel material. Finite element (FE) models created on the basis of the design details of these ratings are illustrated in Figure 3. Table 1 shows design details of initially designed motors for all three ratings.

Item	Unit	Motor 1 *(2 kW, 200 krpm)*	Motor 2 *(5 kW, 24 krpm)*	Motor 3 *(120 kW, 10 krpm)*
Stator outer diameter	mm	44.5	88.06	364.4
Stator inner diameter	mm	23.2	52.08	201.4
Stator back iron depth	mm	4.06	8.77	45
Stator tooth width	mm	3.5	6.82	42
No. of phases	-	3	3	3
No. of poles	-	4	4	4
No. of stator slots	-	12	12	12
Air-gap length	mm	0.5	0.5	0.5
Rotor outer diameter	mm	22.2	51.08	200.4
Core material	-	M19	M19	M19
Type of PM	-	NdFeB35	NdFeB35	NdFeB35

Table 1. Initial design details.

All three different rating motors are designed with the same number of stator slots and three phases of winding distributed in it. The number of rotor poles is also considered to be the same and made of NdFeB type permanent magnet. Permanent magnets are inserted in the rotor core to obtain interior rotor pole arrangement. Neodymium Iron Boron (NdFeB) permanent magnets of 35^{th} grade (i.e. N35) are used with the magnetization in alternately reversing polarity in a spoke-type arrangement to form rotor poles. The stator core, teeth and rotor core were designed using M19 (non-oriented silicon steel) material. M19 material exhibits a saturation level of 1.8 T [25]. The 0.5 mm of air-gap thickness is taken into account for all three ratings. Since large air-gap width will cause weak interaction of stator teeth and flux, the air-gap

thickness is kept small. Average magnetic loading of 0.7 T and slot-loading of 180 A is assumed in all cases. All three initial models consider the space factor of 0.4 and the current density of 6 A/mm^2. Motors are designed with an assumed stator teeth flux density of 1.8 T and stator core flux density of 1.5 T. To compare and analyse performance, initial designs are used as benchmarks.

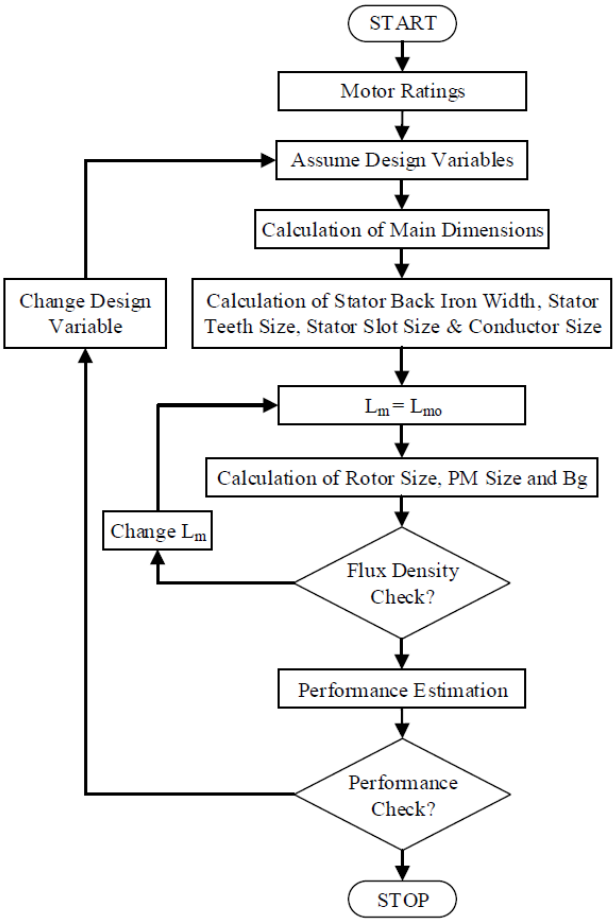

Figure 2. Flowchart for CAD of IPMSM.

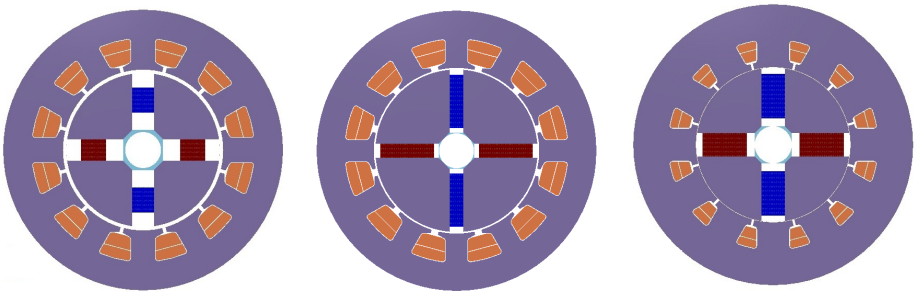

(a) 2 kW motor (b) 5 kW motor (c) 120 kW motor

Figure 3. Initial IPMSM motors with M19 silicon steel material (a) 2 kW motor, (b) 5 kW motor and (c) 120 kW motor.

Design data is used to create finite element models, and meshing is done. The performance results obtained for FEA of the initial models designed using M19 material for core are enlisted in Table 2. Torque profiles and flux density plots are plotted as per the recorded results. Figure 4 represent the torque profile of 2 kW, 200 000 rpm IPMSM obtained from FEA. Figure 5 shows the flux density plot of 2 kW, 200 000 rpm IPMSM. This reference 2 kW, 200 000 rpm IPMSM has average torque of 0.0956 N.m. The actual flux density is close to the assumed flux density in various magnetic sections of the motor. The closeness between actual flux density and assumed flux density validates the sizing of the motor.

Item	Unit	Motor 1 *(2 kW, 200 krpm)*	Motor 2 *(5 kW, 24 krpm)*	Motor 3 *(120 kW, 10 krpm)*
Efficiency	(%)	82.1	88.3	91.2
Losses	kW	0.426	0.657	11.3
Weight	kg	0.2148	2.278	151.6
Average Torque	N.m.	0.0956	1.99	114

Table 2. FEA results of initial models.

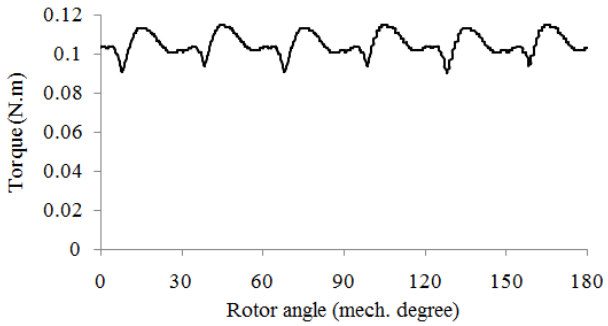

Figure 4. Torque profile of 2 kW, 200 000 rpm reference motor.

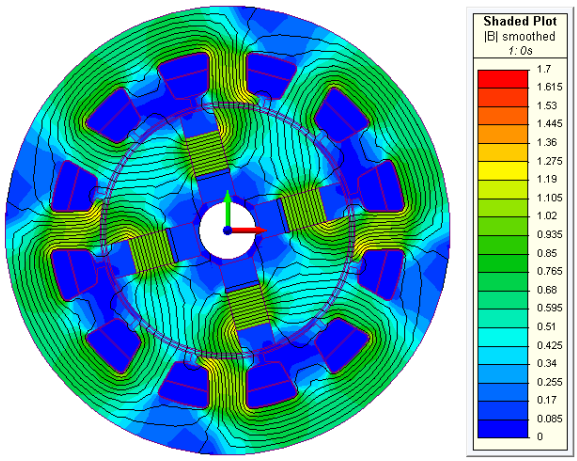

Figure 5. Flux density plot of 2 kW, 200 000 rpm reference motor.

The torque profile and flux density plot of 5 kW, 24 000 rpm IPMSM using M19 material is in Figure 6 and Figure 7, respectively. This 5 kW, 24 000 rpm IPMSM has average torque of 1.99 N.m. It can be observed that the actual flux density is close to the assumed flux density in various magnetic sections of the 5 kW motor.

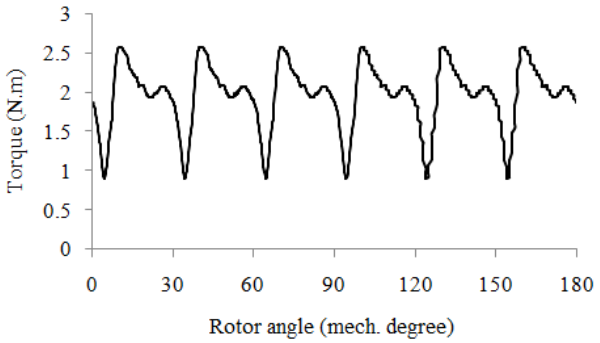

Figure 6. Torque profile of 5 kW, 24 000 rpm reference motor.

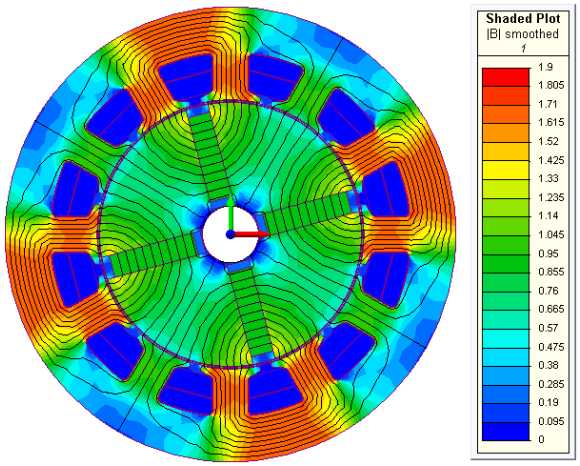

Figure 7. Flux density plot of 5 kW, 24 000 rpm reference motor.

The torque profile and flux density map of the reference 120 kW, 10 000 rpm IPMSM acquired from FEA are shown in Figures 8 and 9, respectively. The average torque of this 120 kW, 10 000 rpm IPMSM is 114 N.m. Similar to the previous two designed motors, the actual flux density is close to the assumed flux density in various magnetic sections of the motor. Close agreement between results obtained from FEA and design considerations validate design methodology.

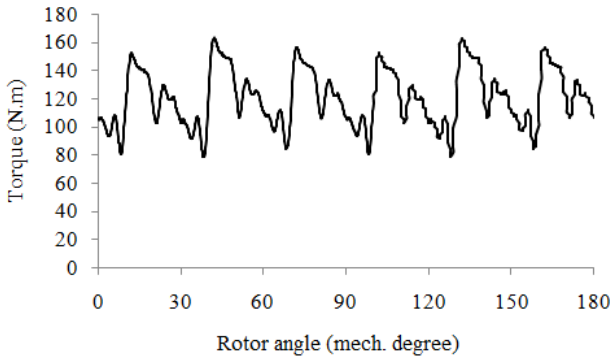

Figure 8. Torque profile of 120 kW, 10 000 rpm reference motor.

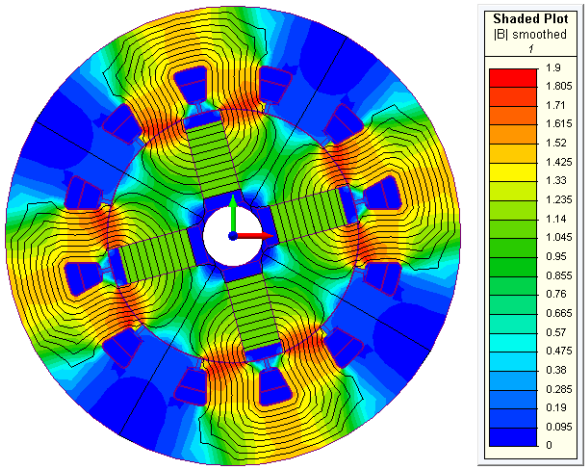

Figure 9. Flux density plot of 120 kW, 10 000 rpm reference motor.

3. Design Improvement of IPMSM

In high-speed applications, the performance of the motor is one of the major concerns. And by reducing the iron losses performance of radial flux, IPMSM can be enhanced. This reduction in iron loss can be achieved with the help of better magnetic materials having higher permissible flux density, higher permeability, and lower specific iron loss. Initially, the motors were designed using M19 silicon steel material with magnetic saturation lies between 1.5 – 1.8 T. With the objective of performance enhancement, all three IPMSM of 2 kW, 200 000 rpm, 5 kW, 24 000 rpm and 120 kW, 10 000 rpm are designed using Hiperco 50A magnetic material. Hiperco 50A is a soft magnetic alloy of iron-cobalt-vanadium with a high value of magnetic saturation (2.3 – 2.4 T), which is greater than that of the M19 material's magnetic saturation point. It also exhibits lower specific iron loss, lower coercive force, and higher permeability.

Figure 10 shows the comparison of the B-H curves of Hiperco 50A and M19 core material. It is clearly observed that Hiperco 50A has a knee point of magnetization at a higher flux density compared to that of M19 material. The comparison between specific iron loss of Hiperco and M19 core at 50 Hz frequency is shown in Figure 11. The curve shows that at 50 Hz frequency and 1.5 T, M19 magnetic material has a specific iron loss of 2.4 W/kg while Hiperco 50A material has a specific iron loss of 1.4 W/kg. Hence, it can be stated that Hiperco 50A material exhibits relatively good properties compared to the M19 material.

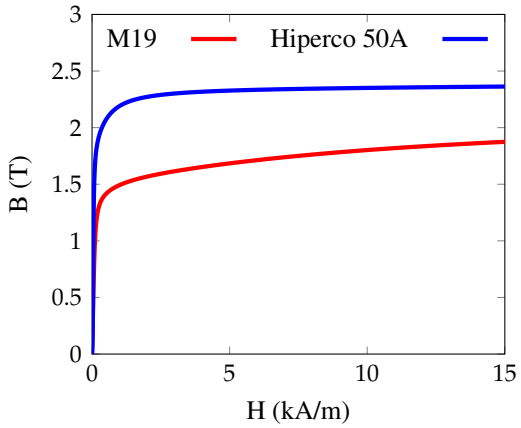

Figure 10. Comparison of the B-H curves of Hiperco 50A and M19 core materials.

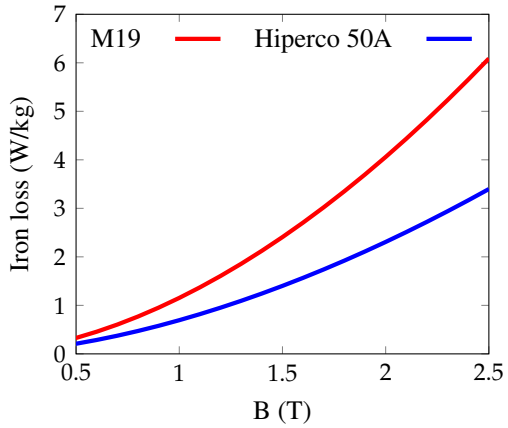

Figure 11. Loss compression of M19 and Hiperco 50A materials for different values of flux density.

Hiperco 50A, a higher-grade material, is used to form the stator core and teeth, whereas the rotor core material is kept unchanged. The Hiperco 50A material has magnetic saturation at 2.3 T and has properties that make it superior, as discussed in Table 3. Applying Hiperco 50A results in lower iron core losses and decreased magneto-motive force drop on the magnetic circuit. This would appear in the lower excitation requirement of IPMSM [26]. Finite element (FE) models of these ratings created based on the design details are shown in Figure 12. The design details of improved motors with Hiperco 50A material used as stator core for all three ratings are shown in Table 4. Dimensions of the improved motors listed are determined based on manual iterations assuming a higher value of flux density in the stator core as Hiperco 50A has high magnetic saturation (2.3 - 2.4 T). High flux density in the stator core is considered to reduce size and weight. During this exercise, the stator slot area is kept the same as the initial design. The width of the NdFeB permanent magnet bars used for designing the rotor poles, length of the air gap, and outer rotor diameter remain untouched and are similar to those of reference model for all three ratings.

Properties (At 20 °C)	M19	HIPERCO 50A
Thermal Conductivity $(W/m \cdot C)$	25	29.8
Mass Density (kg/m^3)	7650	8120
Heat Capacity $(J/kg \cdot C)$	490	420
Loss (W/kg)(at 2 Tesla)	1.93	0.82

Table 3. Materials properties comparison table [27, 28].

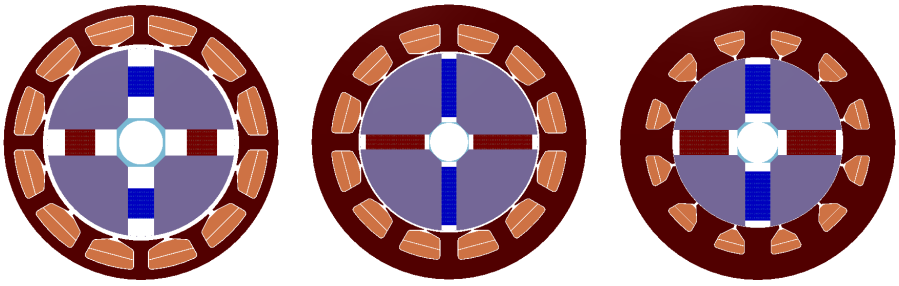

(a) 2 kW motor (b) 5 kW motor (c) 120 kW motor

Figure 12. Improved models of IPMSM using Hiperco 50A material (a) 2 kW motor, (b) 5 kW motor and (c) 120 kW motor.

Item	Unit	Motor 1 *(2 kW, 200 krpm)*	Motor 2 *(5 kW, 24 krpm)*	Motor 3 *(120 kW, 10 krpm)*
Stator outer diameter	mm	34	79	324.4
Stator inner diameter	mm	23.2	52.08	201.4
Stator back iron depth	mm	3.31	5.46	28.5
Stator tooth width	mm	3.5	5	30.5
Slots/Pole/Phase	-	1	1	1
No. of phases	-	3	3	3
No. of poles	-	4	4	4
No. of stator slots	-	12	12	12
Air-gap length	mm	0.5	0.5	0.5
Rotor outer diameter	mm	22.2	51.08	200.4
Stator core material	-	Hiperco 50A	Hiperco 50A	Hiperco 50A
Rotor Core material	-	M19	M19	M19
Type of PM	-	N35	N35	N35

Table 4. Improved design details.

The performance results obtained for FEA of the improved models designed using Hiperco 50A material for core are enlisted in Table 5. Improved Hiperco 50A models offer 88.2%, 92.5%, and 93.3% efficiency for 2 kW, 200 000 rpm, 5 kW, 24 000 rpm and 120 kW, 10 000 rpm rating motors, respectively. Improved torque profiles and flux density plots are generated as per the FEA results obtained with the application of Hiperco 50A material as stator core and teeth material. The torque profile and flux density plot of 2 kW, 200 000 rpm IPMSM obtained from FEA for the improved motor is presented in Figure 13 and Figure 14, respectively.

Item	Unit	Motor 1 *(2 kW, 200 krpm)*	Motor 2 *(5 kW, 24 krpm)*	Motor 3 *(120 kW, 10 krpm)*
Efficiency	(%)	88.2	92.5	93.3
Losses	kW	0.27	0.429	8.51
Weight	kg	0.129	1.847	119.4
Torque	N.m.	0.0953	1.99	114

Table 5. FEA results of improved models.

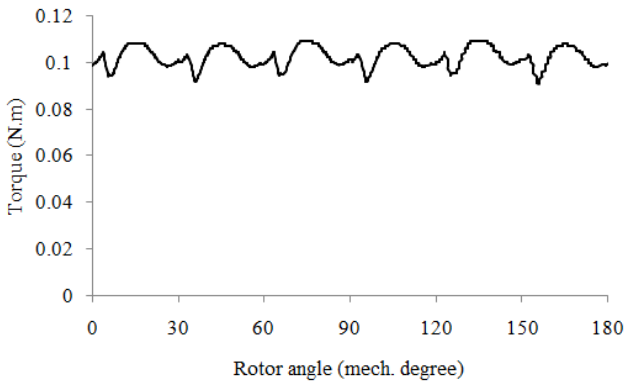

Figure 13. Torque profile of improved 2 kW, 200 000 rpm motor.

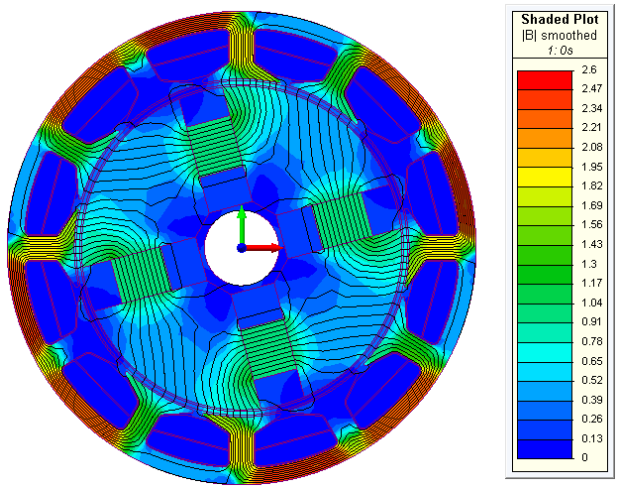

Figure 14. Flux density plot of improved 2 kW, 200 000 rpm motor.

The torque profile and flux density plot for the improved motor with rating 5 kW, 24 000 rpm IPMSM using Hiperco 50A material are shown in Figure 15 and Figure 16, respectively. This 5 kW, 24 000 rpm improved IPMSM has average torque of 1.99 N.m., similar to the initial design. Still, the torque profile is considerably better than that of the initially designed motor with M19 material. It can be observed that the actual flux density is close to the assumed flux density in various magnetic sections of both 2 kW and 5 kW motors.

Figure 17 and Figure 18 represent the improved torque profile and flux density plot of 120 kW, 10 000 rpm IPMSM with Hiperco 50A material obtained from FEA, respectively. This improved 120 kW, 10 000 rpm IPMSM has average torque of 114 N.m. It is observed that the quality of the torque profile of the 120 kW motor is improved as an added advantage of the use of Hiperco 50A. Similar to the previous two designed motors the actual flux density is close to the assumed flux density in various magnetic sections of the motor.

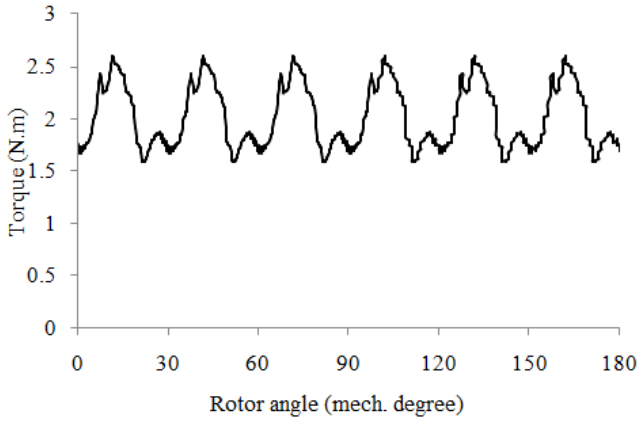

Figure 15. Torque profile of improved 5 kW, 24 000 rpm motor.

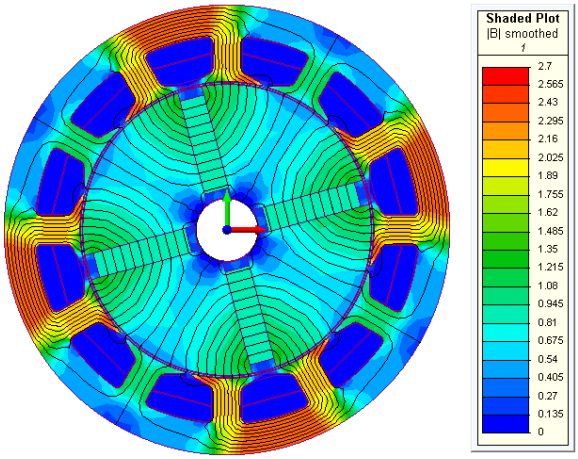

Figure 16. Flux density plot of improved 5 kW, 24 000 rpm motor.

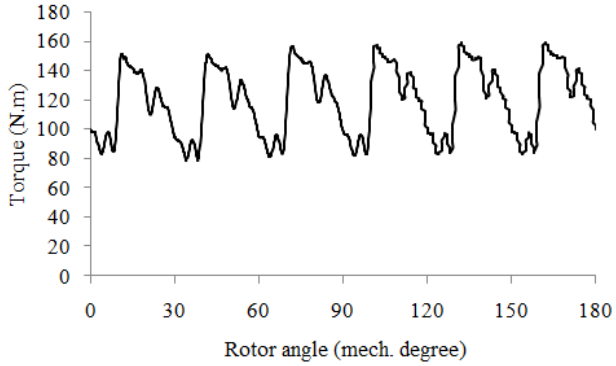

Figure 17. Torque profile of improved 120 kW, 10 000 rpm motor.

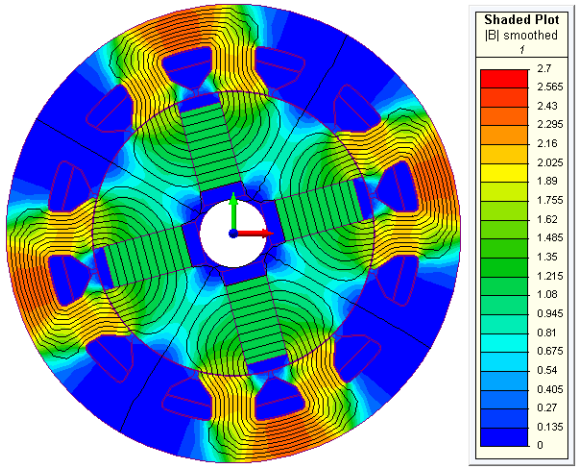

Figure 18. Flux density plot of improved 120 kW, 10 000 rpm motor.

4. Performance Comparison

The comparative analysis of the obtained results of both the initial designs with M19 as stator core material and improved designs with Hiperco 50A as stator core material for all three different ratings is carried out. The performance results comparison is shown in Table 6.

	Motor 1 *(2 kW, 200 krpm)*		Motor 2 *(5 kW, 24 krpm)*		Motor 3 *(120 kW, 10 krpm)*	
Parameter	Initial	Improved	Initial	Improved	Initial	Improved
Efficiency	82.1	88.2	88.3	92.5	91.2	93.3
Losses (kW)	0.426	0.27	0.657	0.429	11.3	8.51
Weight (kg)	0.2148	0.1292	2.278	1.847	151.6	119.4
Torque(N.m.)	0.0956	0.0953	1.99	1.99	114	114

Table 6. Performance comparison.

Efficiency is improved from 82.1% to 88.2%, and weight is reduced from 0.2148 kg to 0.1292 kg in the case of a 2 kW motor. For a 5 kW motor, efficiency is improved from 88.3% to 92.5%, and weight is reduced from 2.278 kg to 1.847 kg. For the motor of 120 kW, rating efficiency is improved from 91.2% to 93.3%, and weight is reduced from 151.6 kg to 119.4 kg. The initial design is considered the reference design for performance comparison. Various parameters like copper losses, core losses, core weight, and PM weight are compared along with the main performance parameters of efficiency and weight. Hiperco 50A material offers less specific iron loss due to its superior magnetic properties; hence a significant reduction in core loss is observed. Comparative analysis of weights and losses of the different motors of 2 kW, 5 kW, and 120 kW rating with M19-based initial designs and Hiperco 50A-based improved designs are shown in Figure 19, Figure 20, and Figure 21, respectively. This comparative analysis validates the effectiveness of the use of Hiperco 50A for performance enhancement of high-speed IPMSM.

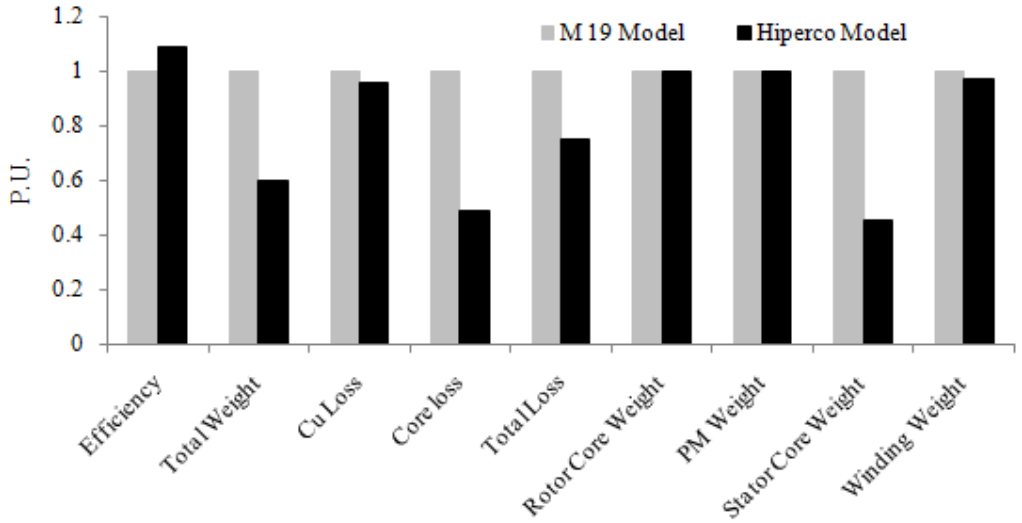

Figure 19. Performance comparison of 2 kW, 200 000 rpm motors.

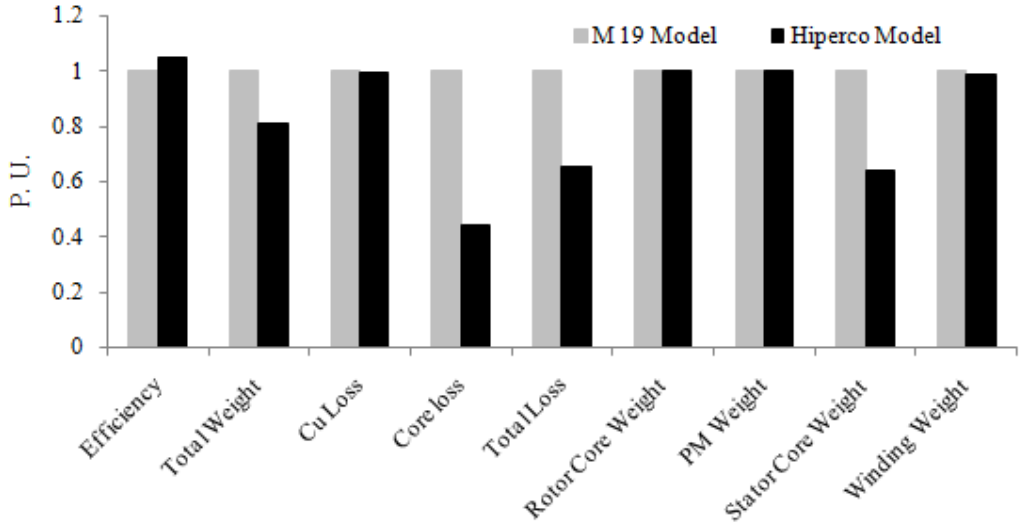

Figure 20. Performance comparison of 5 kW, 24 000 rpm motors.

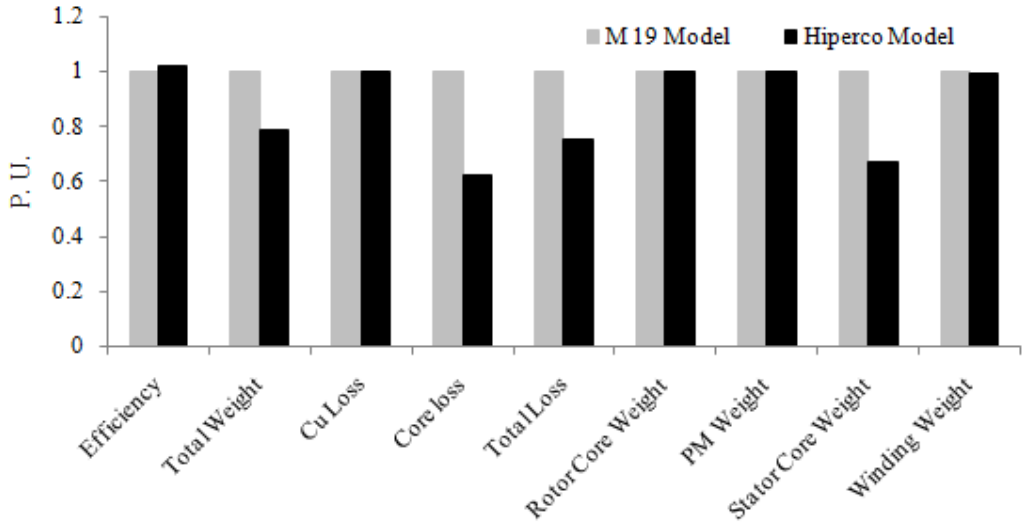

Figure 21. Performance comparison of 120 kW, 10 000 rpm motors.

5. Conclusions

Efficiency improvement and weight reduction of interior permanent magnet synchronous motors are challenges for motor designers. It is very essential to improve efficiency and reduce weight for overall performance enhancement of the system. Hiperco 50A in stator assembly is applied instead of M19 cold-rolled silicon steel material to obtain the reduction in losses, weight, and size of interior permanent magnet synchronous motors. Three standard rating motors are considered in the analysis to assess the effectiveness of the use of Hiperco 50A material on weight reduction, size reduction, and average torque profile in a wide range. The effect of using Hiperco 50A on specific parameters like efficiency and weight of the motor is analyzed with finite element modelling, simulation, and analysis. The overall reduction in losses of 36.61% in 2 kW motor, 34.70% in 5 kW motor, and 24.69% in 120 kW motor is achieved. While considerable weight reduction of 39.85% in 2 kW motor, 18.92% in 5 kW motor and 21.24% in 120 kW motor is also achieved. In all three cases, a significant increase in efficiency and a decrease in weight are

achieved with very minor changes in average torque. This proposed method is practically implementable as it does not increase manufacturing complexity. The results confirm that the application of Hiperco 50A material is helpful in the performance enhancement of IPMSM. Hiperco can also be effectively used to improve the performance of other types of high-speed electrical motors.

Funding: This research received no external funding.

Author contributions: Author Contribution: Conceptualization, Tanuj Jhankal and Amit N. Patel; Methodology, Tanuj Jhankal and Amit N. Patel; Software, Tanuj Jhankaland Amit N. Patel; Validation, Tanuj Jhankal and Amit N. Patel; Formal Analysis, Tanuj Jhankal and Amit N. Patel; Investigation, Tanuj Jhankal and Amit N. Patel; Resources, Tanuj Jhankal and Amit N. Patel; Data Curation, Tanuj Jhankal and Amit N. Patel; Writing – Original Draft Preparation, Tanuj Jhankal; Writing – Review & Editing, Tanuj Jhankal and Amit N. Patel; Supervision, Amit N. Patel.

Disclosure statement: The authors declare no conflict of interest.

References

[1] Meng Si, Xiang Yu Yang, Shi Wei Zhao, and Sheng Gong. Design and analysis of a novel spoke-type permanent magnet synchronous motor. *IET Electric Power Applications*, 10(6):571–580, 2016.

[2] Qiping Shen, Ziyao Zhou, Shan Li, Xinglin Liao, Tao Wang, Xiaorong He, and Jingshan Zhang. Design and analysis of the high-speed permanent magnet motors: A review on the state of the art. *Machines*, 10(7), 2022.

[3] Tianran He, Ziqiang Zhu, Fred Eastham, Yu Wang, Hong Bin, Di Wu, Liming Gong, and Jintao Chen. Permanent magnet machines for high-speed applications. *World Electric Vehicle Journal*, 13(1), 2022.

[4] Zheng Li, Pengju Wang, Libo Liu, Qianqian Xu, Shuai Che, Lucheng Zhang, Shenhui Du, Hongjie Zhang, and Hexu Sun. Loss calculation and thermal analysis of ultra-high speed permanent magnet motor. *Heliyon*, 8(11):e11350, 2022.

[5] Nuwantha Fernando and Fuad Hanin. Magnetic materials for electrical machine design and future research directions: A review. In *2017 IEEE International Electric Machines and Drives Conference (IEMDC)*, pages 1–6, 2017.

[6] Yannis Karnavas and Ioannis Chasiotis. Influence of soft magnetic materials application to squirrel cage induction motor design and performance. *Engineering Journal*, 21:193–206, 01 2017.

[7] M. Ishida, N. Shiga, and K. Sadahiro. Improvement of motor performance by use of high-efficiency electrical steels. *Kawasaki Steel Technical Report*, pages 39–46, 03 2003.

[8] Jiang Xintong, Xing Jingwei, Li Yong, and Lu Yongping. Theoretical and simulation analysis of influences of stator tooth width on cogging torque of bldc motors. *IEEE Transactions on Magnetics*, 45(10):4601–4604, 2009.

[9] Xiao Ge, Z. Q. Zhu, Graham Kemp, David Moule, and Connel Williams. Optimal step-skew methods for cogging torque reduction accounting for three-dimensional effect of interior permanent magnet machines. *IEEE Transactions on Energy Conversion*, 32(1):222–232, 2017.

[10] D.C. Hanselman. *Brushless Permanent-magnet Motor Design*. New Horizons in Comparative Politics. McGraw-Hill, 1994.

[11] T. H. Panchal, R. M. Patel, and A. N. Patel. Efficiency improvement of radial flux permanent magnet brushless dc motor using hiperco magnetic material. *International Journal of Engineering Trends and Technology*, 69(5):57–61, 2021.

[12] J.R. Hendershot and T.J.E. Miller. *Design of Brushless Permanent-magnet Motors*. Magna physics publications. Magna Pysics Pub., 1994.

[13] Mohammad Ehsan Abdollahi, Ahsan Zahid, Nir Vaks, and Berker Bilgin. Switched reluctance motor design for a light sport aircraft application. *Machines*, 11(3), 2023.

[14] Andreas Krings, Marco Cossale, Alberto Tenconi, Juliette Soulard, Andrea Cavagnino, and Aldo Boglietti. Magnetic materials used in electrical machines: A comparison and selection guide for early machine design. *IEEE Industry Applications Magazine*, 23(6):21–28, 2017.

[15] Xiaolong Zhang and Kiruba Sivasubramaniam Haran. High-specific-power electric machines for electrified transportation applications-technology options. In *2016 IEEE Energy Conversion Congress and Exposition (ECCE)*, pages 1–8, 2016.

[16] Nuwantha Fernando, Gaurang Vakil, Puvan Arumugam, Emmanuel Amankwah, Chris Gerada, and Serhiy Bozhko. Impact of soft magnetic material on design of high-speed permanent-magnet machines. *IEEE Transactions on Industrial Electronics*, 64(3):2415–2423, 2017.

[17] M. Ramkumar and K. Latha. Analysis of maximizing the power output of switched reluctance generator using different core materials. *Advances in Materials Science and Engineering*, 2023:1–10, 01 2023.

[18] Mohammad Ehsan Abdollahi, Nir Vaks, and Berker Bilgin. A multi-objective optimization framework for the design of a high power-density switched reluctance motor. In *2022 IEEE Transportation Electrification Conference & Expo (ITEC)*, pages 67–73, 2022.

[19] Andreas Krings, Aldo Boglietti, Andrea Cavagnino, and Steve Sprague. Soft magnetic material status and trends in electric machines. *IEEE Transactions on Industrial Electronics*, 64(3):2405–2414, 2017.

[20] Pedro P. C. Bhagubai, António C. Cardoso, and João F. P. Fernandes. Cobalt iron core impact on optimal design of an interior permanent magnet synchronous motor for competition electric vehicle. In *2020 2nd Global Power, Energy and Communication Conference (GPECOM)*, pages 158–163, 2020.

[21] P.R. Upadhyay and K.R. Rajagopal. Fe analysis and computer-aided design of a sandwiched axial-flux permanent magnet brushless dc motor. *IEEE Transactions on Magnetics*, 42(10):3401–3403, 2006.

[22] J.F. Gieras and M. Wing. *Permanent Magnet Motor Technology : Design and Applications*. Magna physics publications. CRC Press Bocan Ratan FL, 2002.

[23] P.R. Upadhyay and K.R. Rajagopal. Fe analysis and cad of radial-flux surface mounted permanent magnet brushless dc motors. *IEEE Transactions on Magnetics*, 41(10):3952–3954, 2005.

[24] Md Mojibur Rahaman and K. S. Sandhu. Energy efficient magnetic materials for electrical machines. In *2019 5th International Conference on Advanced Computing & Communication Systems (ICACCS)*, pages 642–646, 2019.

[25] Keun-Young Yoon and Soo-Whang Baek. Performance improvement of concentrated-flux type ipm pmsm motor with flared-shape magnet arrangement. *Applied Sciences*, 10:6061, 09 2020.

[26] Karel Hruska, Jan Laksar, and Jan Sobra. The determination of iron core loss characteristics of special electrical steel types. In *2018 18th International Conference on Mechatronics - Mechatronika (ME)*, pages 1–6, 2018.

[27] AK Steel. Selection of electrical steel for magnetic cores, 2007.

[28] Carpenter Technology. Cartech® hiperco® 50a alloy, 2020.